Phase diagrams of the Ashkin-Teller Model on the Cayley Tree

J. M. de Araújo and F. A. da Costa
Departamento de Física Teórica e Experimental,
Universidade Federal do Rio Grande do Norte,
Campus, Caixa Postal 1641,
59072-970 Natal, Rio Grande do Norte, Brazil

Received February 12, 1997

We study the Ashkin-Teller model on a Cayley tree of finite coordination z as a mapping problem. The stability analysis of the fixed points is used to obtain set of phase diagrams as a function of z. Our treatment reveals a rich variety of distinct topologies obtained for these diagrams.

I. Introduction

The Ashkin-Teller model [1] may be considered as two superposed Ising models which are coupled by a four-spin interaction term [2]. The Hamiltonian is given by

$$\mathcal{H} = -J_2 \sum_{(ij)} (\sigma_i \sigma_j + \tau_i \tau_j) - J_4 \sum_{(ij)} \sigma_i \sigma_j \tau_i \tau_j , \qquad (1)$$

where σ_i, τ_i are classical Ising spins variables taking the values ± 1 on each lattice site, J_2 (J_4) denotes the strenght of the two (four)-spin interactions, and (ij) denotes a summation over all distincts pairs of nearest-neighbor sites on a lattice.

This model has been studied on a square lattice and the structure of its phase diagram is well understood on the basis of exact results [3, 4]. Recently an analysis of the dynamical aspects of this model on a square lattice was reported [5]. The quantum Ashkin-Teller chain [6] has also been investigated mainly with respect to its conformal invariance aspects [7]. There were also some attempts to relate the quantum Ashkin-Teller chain to the Haldane conjecture [8] through an equivalence with a spin$-1/2$ alternating Heisenberg chain [9, 10]. In three dimensions, however, our knowledge of the phase diagrams relies on approximated techniques, including mean-field calculations, renormalization group treatments, series analysis and Monte Carlo method [11, 12, 13]. The phase diagram thus obtained shows a variety of multicritical points. However, these approximated results are mainly concerned with the simple cubic lattice. For other lattices, however, competition between J_2 and J_4 may give rise to distinct phase diagrams depending on the lattice topology. We thus decided to investigate this point using an approach that, despite its simplicity, is able to account for the lattice structure.

In this work we use an iterative procedure to determine the local properties of the Ashkin-Teller model on a Cayley tree. We are mainly interested in the fixed points of a three-dimensional mapping generated by this scheme. For a Cayley tree of coordination z these fixed points corresponds to the Bethe-Peierls approximation. The stability analysis of these fixed points are then used to obtain the phase diagrams as a function of the coordination number z.

This paper is organized as follow. In Section II we formulate the Ashkin-Teller model on a Cayley tree with arbitrary coordination number z. We derive the basic equations for an exact three-dimensional mapping. In Section III we discuss the stability criteria

for the fixed point solutions of the mapping along with a presentation of the phase diagrams obtained according to these criteria. Finally, in Section IV we present some concluding remarks.

II. The Ashkin-Teller model on a cayley tree

The Cayley tree is a lattice with no closed loops and a fixed coordination number z (Fig. 1 shows a Cayley tree with $z = 3$ and four generations). The outermost generation is considered as the first shell, the next generation as the second shell and so on. Due to its cycle-free structure it is possible to perform a partial summation decimation over the spins on the outermost generation. Then we can repeat this process on the next generation. In this way we obtain recursive relations between efective fields acting on successive shells [14]. For instance, considering a site on the $(\ell+1)$–th shell connected to $r = z - 1$ sites on the ℓ–th shell we have

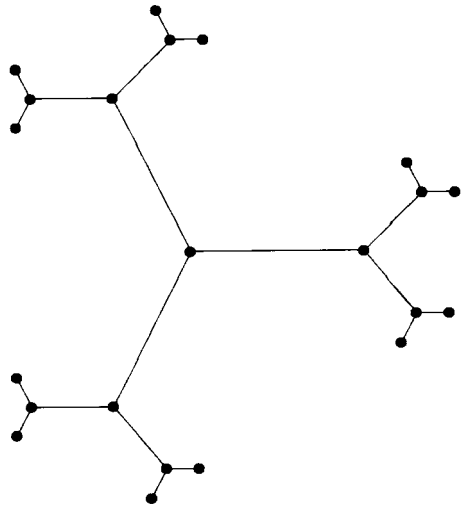

Figure 1. Three generations of a Cayley tree with coordination $z = 3$.

$$\sum_{\{\sigma_i,\tau_i\}} \exp[(K_2\sigma + H_{1,\ell})\sum_{i=1}^{r}\sigma_i + (K_2\tau + H_{2,\ell})\sum_{i=1}^{r}\tau_i + (K_4\sigma\tau + H_{4,\ell})\sum_{i=1}^{r}\sigma_i\tau_i]$$

$$= 8^r[\cosh(K_2\sigma + H_{1,\ell})\cosh(K_2\tau + H_{2,\ell})\cosh(K_4\sigma\tau + H_{4,\ell}) + \sinh(K_2\sigma + H_{1,\ell})\sinh(K_2\tau + H_{2,\ell})\sinh(K_4\sigma\tau + H_{4,\ell})]^r \quad (2)$$

where $K_a = J_a/k_BT$ $(a = 2, 4)$, k_B is the Boltzmann constant and T is the absolute temperature. The *effective* fields $H_{1,\ell}$, $H_{2,\ell}$ and $H_{4,\ell}$ are generated by the decimation process. Eq. (2) can be written as a single-site effective partition function

$$\mathcal{Z}_{\ell+1}(\sigma,\tau) = A\exp[H_{1,\ell+1}\sigma + H_{2,\ell+1}\tau + H_{4,\ell+1}\sigma\tau], \quad (3)$$

where $H_{1,\ell+1}, H_{2,\ell+1}$ and $H_{4,\ell+1}$ are the new effective fields acting on the $(\ell+1)$–*th* shell. From Eqns. (2) and (3) it is straightforward to obtain the recursion relation between successive effective fields. However, it is convenient to introduce new variables defined by

$$m_{1,\ell} = \frac{\sum_{\{\sigma,\tau=\pm1\}}\sigma\mathcal{Z}_\ell(\sigma,\tau)}{\mathcal{Z}_\ell}, \quad (4)$$

$$m_{2,\ell} = \frac{\sum_{\{\sigma,\tau=\pm1\}}\tau\mathcal{Z}_\ell(\sigma,\tau)}{\mathcal{Z}_\ell}, \quad (5)$$

$$q_\ell = \frac{\sum_{\{\sigma,\tau=\pm1\}}\sigma\tau\mathcal{Z}_\ell(\sigma,\tau)}{\mathcal{Z}_\ell}, \quad (6)$$

where

$$\begin{aligned} \mathcal{Z}_\ell &= \mathcal{Z}_\ell(+1,+1) + \mathcal{Z}_\ell(+1,-1) \\ &+ \mathcal{Z}_\ell(-1,+1) + \mathcal{Z}_\ell(-1,-1). \end{aligned} \tag{7}$$

These variables may be seen as local magnetization (m_1 and m_2) and polarization (q). The relation between these parameters and the effective fields can be easily obtained. For instance, on the $(\ell+1)$–*th* shell we have

$$m_{1,\ell+1} = \frac{\tanh H_{1,\ell+1} + \tanh H_{2,\ell+1} \tanh H_{4,\ell+1}}{D}, \tag{8}$$

$$m_{2,\ell+1} = \frac{\tanh H_{2,\ell+1} + \tanh H_{1,\ell+1} \tanh H_{4,\ell+1}}{D}, \tag{9}$$

$$q_{\ell+1} = \frac{\tanh H_{4,\ell+1} + \tanh H_{1,\ell+1} \tanh H_{2,\ell+1}}{D}, \tag{10}$$

where

$$D = 1 + \tanh H_{1,\ell+1} \tanh H_{2,\ell+2} \tanh H_{4,\ell+1} \ . \tag{11}$$

On the other hand the effective fields on the $(\ell+1)$–*th* shell may be expressed in terms of the local magnetization on the preceeding shell by

$$H_{1,\ell+1} = \frac{r}{2} \tanh^{-1} \left[\frac{2\alpha(m_{1,\ell} - \gamma m_{2,\ell} q_\ell)}{1 + \alpha^2 m_{1,\ell}^2 - \alpha^2 m_{2,\ell}^2 - \gamma^2 q_\ell^2} \right], \tag{12}$$

$$H_{2,\ell+1} = \frac{r}{2} \tanh^{-1} \left[\frac{2\alpha(m_{2,\ell} - \gamma m_{1,\ell} q_\ell)}{1 - \alpha^2 m_{1,\ell}^2 + \alpha^2 m_{2,\ell}^2 - \gamma^2 q_\ell^2} \right], \tag{13}$$

$$H_{4,\ell+1} = \frac{r}{2} \tanh^{-1} \left[\frac{2(\gamma q_\ell - \alpha^2 m_{1,\ell} m_{2,\ell})}{1 - \alpha^2 m_{1,\ell}^2 - \alpha^2 m_{2,\ell}^2 + \gamma^2 q_\ell^2} \right], \tag{14}$$

where we have introduced the variables

$$\alpha = \frac{t_2 + t_2 t_4}{1 + t_2^2 t_4}, \quad \gamma = \frac{t_4 + t_2^2}{1 + t_2^2 t_4}, \tag{15}$$

and

$$t_i = \tanh(J_i / k_B T), \quad (i = 2, 4). \tag{16}$$

Eqns. (8) and (12) define together a three-dimensional mapping. Given a set of parameters (temperature, coupling constants and coordination number) and a set of boundary conditions (initial conditions), we iterate the mapping and look for its fixed points, i.e., for points such that

$$(m_{1,\ell+1}, m_{2,\ell+1}, q_{\ell+1}) = (m_{1,\ell}, m_{2,\ell}, q_\ell) = (m_1^*, m_2^*, q^*),$$

for some $\ell \geq L > 0$. These fixed points, if they do exist, are then associated with the solutions deep within the Cayley tree. It has been shown that these solutions correspond to the so-called Bethe-Peierls approximation on a physical lattice with the same coordination number [3].

III. The phase diagrams

In this section we present our results for the phase diagrams as the coordination number is varied. We will use the stability analysis of the fixed points of the mapping to obtain the phase diagrams in the variables

$$\theta = k_B T/J_2(z-1) \quad \text{and} \quad p = J_4/J_2. \tag{17}$$

A fixed point is considered stable if all eigenvalues Λ_i, for $i = 1, 2, 3$, of the Jacobian matrix

$$\mathbf{M} = \begin{pmatrix} \frac{\partial m_{1,\ell+1}}{\partial m_{1,\ell}} & \frac{\partial m_{1,\ell+1}}{\partial m_{2,\ell}} & \frac{\partial m_{1,\ell+1}}{\partial q_\ell} \\ \frac{\partial m_{2,\ell+1}}{\partial m_{1,\ell}} & \frac{\partial m_{2,\ell+1}}{\partial m_{2,\ell}} & \frac{\partial m_{1,\ell+1}}{\partial q_\ell} \\ \frac{\partial q_{\ell+1}}{\partial m_{1,\ell}} & \frac{\partial q_{\ell+1}}{\partial m_{2,\ell}} & \frac{\partial q_{\ell+1}}{\partial q_\ell} \end{pmatrix} \tag{18}$$

evaluated at the fixed point are less than one in absolute values. The stability boundary of a fixed point is defined by

$$|\Lambda|_{max} = 1, \tag{19}$$

for the largest eigenvalue in absolute value. Each fixed point is associated with a thermodynamic phase and a corresponding region of stability in the phase diagram. It may happen that different regions of stability overlap between themselves. In this case the phase which is realized deep within the tree depends on the boundary condition. Physically the overlap between regions of stability indicates the existence of a first-order transition. It turns out that to determine the loci of the first-order transitions we need a free energy functional associated with the corresponding fixed points. We have not made any attempt to obtain such a functional since we are interested only in the qualitative phase diagrams that may result. However, we remark that a free energy functional could be obtained by standard methods [3, 14, 16].

Paramagnetic fixed point

The paramagnetic (trivial) fixed point is given by $m_1^* = m_2^* = q^* = 0$ and it always exists for any value of z, p, and θ. Their stability boundaries can be obtained analitically. Figs. 2 through 5 show these boundaries as the lines L_1, L_2 and L_5. Their equation are given by

$$p = -r\theta \tanh^{-1}\left(\frac{1+rt_1^2}{r+t_1^2}\right), \quad \text{for } L_1,$$

$$p = r\theta \tanh^{-1}\left(\frac{1-rt_1}{rt_1-t_1^2}\right), \quad \text{for } L_2,$$

$$p = r\theta \tanh^{-1}\left(\frac{1-rt_1^2}{r-t_1^2}\right), \quad \text{for } L_5.$$

For $z = 3$ and 4 the lines L_1 and L_2 merge together at the multiphase point $\theta = 0$, $p = -1$ as seen in Figs. 2, 3. For $z \geq 5$ they still meet at $p = -1$ but with $\theta \neq 0$. This common point is denoted by J on Figs. 4, 5. We note also that for any value of the coordination number the lines L_2 and L_5 meet together at the four-state Potts point $p = 1$. Finally we mention that L_1 is the sole border between the paramagnetic and the $\langle\sigma\tau\rangle_{AF}$ (see below) phases. Thus we conclude that the transitions between these phases are always continuous, irrespective of the coordination number.

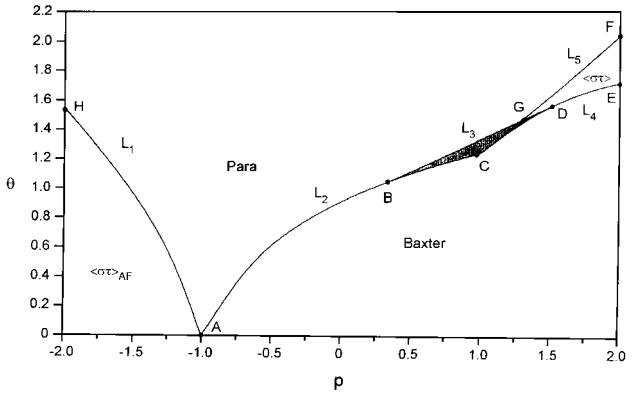

Figure 2. Phase diagram on the Cayley tree with $z = 3$. In the shaded area $BCGB$ there exists two stable fixed points corresponding to the paramagnetic and the Baxter phases, whereas inside $CDGC$ there are also two stable fixed points associated with the $\langle\sigma\tau\rangle$ and the Baxter phases. We note that B and D are *tricritical* points. This general behavior remains valid on the next phase diagrams.

Non-trivial fixed points

Depending on the coordination number we can find up to five distincts non-trivial fixed points. As noted before [13], each of them corresponds to a different phase of the original model and are given by

$$
\begin{aligned}
&m_1^* = m_2^* = 0, q \neq 0 && \text{(Ising phase)},\\
&m_1^* = m_2^* \neq 0, q \neq 0 && \text{(Baxter phase)},\\
&m_1^* \neq 0, m_2^* = q = 0 && (\langle\sigma\rangle \text{ phase}),\\
&m_1^* \neq m_2^* \neq 0, q \neq 0 && \text{(Asymmetric Baxter phase)},
\end{aligned}
$$

and a cycle two fixed point

$$(0,0,q^*) \leftrightarrow (0,0,-q^*) \quad (\langle\sigma\tau\rangle_{AF} \text{ phase}).$$

The stability boundaries of these fixed points have been determined numerically. Given a point (p,θ) on the phase diagram we choose an initial condition and iterate the mapping. When the fixed point is attained we then compute the eigenvalues of the stability matrix. For the $\langle\sigma\tau\rangle_{AF}$ we must take a product of two matrices, one for $(0,0,q^*)$ and another for $(0,0,-q^*)$. The stability criterion (19) still holds in this case. Let us discuss some representative phase diagrams thus obtained.

Case $z = 3$ Fig. 2 shows the phase diagram for $z = 3$. We note the existence of three phases besides the already discussed paramagnetic phase. The $\langle\sigma\tau\rangle_{AF}$ phase shares a common border L_1 with the paramagnetic one. Hence L_1 is a continuous-transition line. The Baxter phase is bordered from above by the lines L_2, L_3 and L_4 along the points A, B, G, D and E. The $\langle\sigma\tau\rangle$ phase stability region is bordered by L_4 (from point C to E) and L_5. There are two contiguous overlapping regions. Inside the triangular shaped area $BCGB$ there are two kinds of stable fixed points corresponding to the paramagnetic and Baxter phases. These fixed points also correspond to Bethe lattice solutions [3, 14]. In a standard procedure we compute a free energy density for each solution and decide which phase is thermodynamically stable [13, 15, 16]. However, we will refrain our analysis to the model on a Cayley tree without refering to any free energy density. Hence, we conclude that a first-order transition line, meeting at point B with the continuous-transition line L_2, is located within this region. Hence B is a *tricritical* point. Analogously, whithin the region $CDGC$ there is a presence two stable fixed points associated with the Baxter and $\langle\sigma\tau\rangle$ phases. By the same token we conclude that a first-order transition line between these phases exists inside the above mentioned region. Thus D is also a tricritical point. Finally, there is a *critical endpoint* somewhere along the line GC as two distinct first-order transition lines meets a continous-transition line (L_5). From a qualitative point of view, the structure of the phase diagram does not change as we vary the coordination number z, as long as we consider $p > 0$. In fact, this picture already reproduce the well-known mean-field results [11, 12, 13]. Therefore, we will focus on the $p < 0$ side on the next diagrams.

Case $z = 4$ In addition to the phases already presented in the previous case, the $\langle\sigma\rangle$ is also found as shown in Fig. 3. This phase goes continuously into the paramagnetic phase as we cross L_2. However, in crossing the line L_6 it goes to the Baxter phase with jumps on the order parameters m_1, m_2 and q. This situation is different from what we have discussed so far due to the absence of an overlap between the regions of stability. Based on what was found previously for the infinite-coordination limit [13] we conclude that the line

L_6 is a first-order transition one and consequently I is a bicritical point. We did not find any evidence of the asymmetric Baxter phase.

Case $z = 5$ In this case we found the same phases as for $z = 4$. However, there appears an overlap between the regions of stability of the phases $\langle\sigma\tau\rangle_{AF}$ and $\langle\sigma\rangle$. This overlap is shown in Fig. 4 as a shaded region between lines L_7 and L_8. Therefore, a first-order transition line between the corresponding phases lies within the shaded area. Hence, J is another bicritical point.

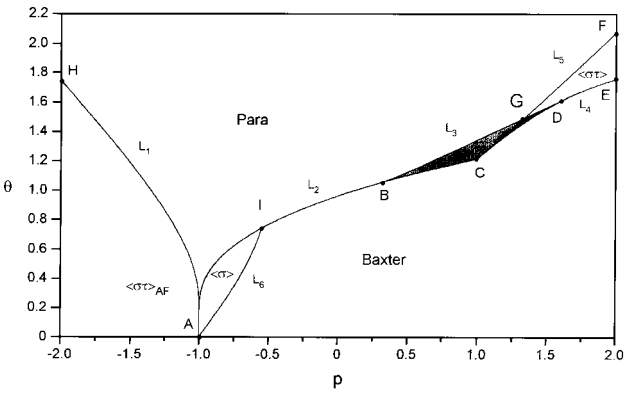

Figure 3. For $z = 4$ there appears an additional phase $\langle\sigma\rangle$ for $p < 0$. The line L_6 is a first-order transition one whereas I is a *bicritical* point.

Case $z = 16$ This phase diagram is qualitatively similar to the infinite-coordination limit [13]. In addition to the phases previously found, the asymmetric Baxter phase is also presented. This new phase is bounded by the lines L_6 and L_9 shown in Fig. 5. We notice that these lines do cross each other before reaching the point I. Due to numerical roundoffs its very difficult to locate precisely the crossing point K for low coordination numbers. In analogy with previous results [13] we conclude that a new bicritical point is associated with the crossing point K. Its worth mentioning that the asymmetric Baxter phase is already found for $z = 7$. However, its stability region is too narrow within the scale settled by the others phases.

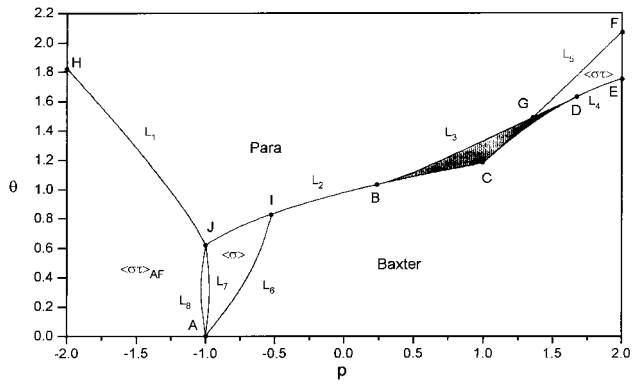

Figure 4. Besides the caracterists of the previous case the phase diagram for $z = 5$ shows another region between L_7 and L_8 where there exists both a stable cycle of period two and a stable fixed point corresponding to the $\langle\sigma\tau\rangle_{\mathrm{AF}}$ and to the $\langle\sigma\rangle$ phases, respectively. There is a first-order transition line bordering these phases that goes from the *multiphase* point A to the *bicritical* point J.

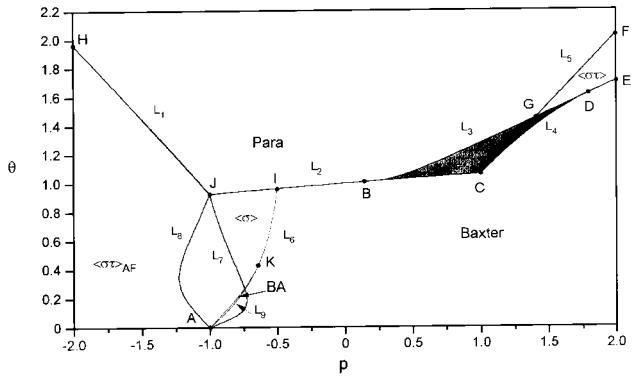

Figure 5. In the $z = 16$ we can note the existence of a very tiny region (BA) where the *asymmetric* Baxter phase sets in. This phase is separated from the $\langle\sigma\rangle$ and the Baxter phase by continuous transition lines meeting at the common *bicritical* point K. This phase diagram has already the same topology of the mean-field (infinite coordination limit) case.

IV. Conclusions

We have studied the Ashkin-Teller model on a Cayley tree of coordination number z as a three-dimensional mapping. The fixed points of this mapping corresponds to the solution on a Bethe lattice with the same coordination number. Several phase diagrams have been shown for representative values of z. These phase diagrams may be seen as a mean-field-like approximation for Bravais lattices with the same coordination number. However, thanks to our knowledge of the two-dimensional model on a square lattice [3], this

approximation should be interpreted with some caution. For $z = 3$, which should correspond to an approximation to the square lattice, we find two tricritical points and one critical endpoint that are not realized on the square lattice. As another instance, for $z = 6$, which is completely similar to the $z = 5$ case, there is no distinction between the triangular and the simple cubic lattices. In this case, we believe that our results are a better guide to the simple cubic lattice due to its higher dimensionality. Finally, its worth to notice that the asymmetric Baxter phase is not presented for $z = 6$, in desagreement with previous analysis [13].

Acknowledgments

We would like to thank A.M. Mariz and S.R. Salinas for useful comments. We acknowledge partial financial support from Consellho Nacional de Desenvolvimento Científico e Tecnológico (CNPq).

References

[1] J. Ashkin and E. Teller, Phys. Rev. **64**, 178 (1943).

[2] C. Fan, Phys. Lett. A **39**, 136 (1972).

[3] R. J. Baxter, *Exactly Solved Models in Statistical Mechanics*, Academic Press, London, 1982.

[4] B. Nienhuis, in *Phase Transitions and Critical Phenomena*, vol. 11, C. Domb and J.L. Lebowitz, eds. Academic Press, London, (1987).

[5] S. Wiseman and E. Domany, Phys. Rev. E **48**, 4080 (1993).

[6] M. Kohmoto, M. den Nijs, and L.P. Kadanoff, Phys. Rev. B **24**, 5229 (1981).

[7] P. Christe and M. Henkel, *Introduction to Conformal Invariance and Its Applications to Critical Phenomena*, Springer-Verlag, Berlin, (1993).

[8] F.D.M. Haldane, Phys. Lett. **93A**, 464 (1983); Phys. Rev. Lett. **50**, 1153 (1983).

[9] K. Hida, Phys. Rev. B **45**, 2207 (1992).

[10] M. Yamanaka, Y. Hatsugai, and M. Kohmoto, Phys. Rev. B **50**, 559 (1994).

[11] R. V. Ditzian, J. R. Banavar, G. S. Grest, and L. P. Kadanoff, Phys. Rev. B **22**, 2542 (1980).

[12] P. L. Christiano and S. G. Rosa, Jr., Phys. Rev. B **33**, 5107 (1986).

[13] F. A. da Costa, M. J. de Oliveira and S. R. Salinas, Phys. Rev. B **36**, 7163 (1987).

[14] C. J. Thompson, J. Stat. Phys. **27**, 441 (1982).

[15] A.Z. Akheyan and N.S. Ananikian, J. Phys. A: Math. Gen. **29**, 721 (1996).

[16] P.D. Gujrati, Phys. Rev. Lett. **74**, 809 (1995).